이학석사학위논문

Ensemble ENSO prediction based on various perturbation methods

다양한 섭동기법을 이용한 앙상블 ENSO 예측

2013년 2월

서울대학교 대학원
협동과정 계산과학전공
윤 지 로

Abstract

Ensemble ENSO prediction based on various perturbation methods

Yun, Jiro

Computational Science and Technology

The Graduate School

Seoul National University

Hindcast seasonal predictions of El Niño-Southern Oscillation (ENSO) are performed using Seoul National University coupled general circulation model (SNU CGCM) for 20 boreal summers of 1991 to 2010. Fourteen different initial conditions are made with lagged average forecasting (LAF), bred vector (BV) and empirical singular vector (ESV). Six LAF ensemble members are generated with forecasts started from 1 to

6 days lagging the actual forecast day. With breeding method, three initial conditions are made using three different breeding intervals (1, 3 and 6 months), and their mirror images are also generated. The other two initial conditions are generated by ESV, which is constructed based on six-month lag between thermocline depth and sea surface temperature (SST).

To compare the predictabilities of the initialization methods, correlation skill of Nino indices are calculated. The results show that both BV and ESV outperform LAF. Among BVs, forecast with one pair of 3-month rescaling BV (BV3) is best especially in the central to western Pacific. To understand the characteristics related to the prediction skill, SST initial perturbation is composited during El-Niño years. The initial perturbation pattern of BV3 reflects warm temperature perturbation over cold tongue area. Even though similar perturbation patterns are also captured by 1-month rescaling BV (BV1) and 6-month rescaling BV (BV6), they are either concentrated in the eastern Pacific (BV1)

or too vague (BV6).

BV perturbations are superior to ESV perturbations for short lead time, but as prediction goes on the run with ESV shows the most outstanding performance. One reason is that spread to error ratio of ESV is approximately 4 times larger than that of BV for long lead times.

When the prediction with BV3 and that with ESV are ensemble averaged, the inferiority of ESV for short lead time is overcome, but no dramatic improvement is observed before and after ensemble averaging.

Keywords

ENSO, prediction, lagged average forecasting, bred vector, empirical singular vector, coupled GCM

Student number: 2009-22978

Contents

Table and Figure Captions

You can see the original figures and table at

blog.daum.net/jirosmart or here :

1. Introduction

Inaccurate initial conditions, along with imperfect models, bring errors in prediction. Initial conditions are constructed by adding small perturbations to the analysis. For decades a number of perturbation methodologies have been developed such as the breeding method (Toth and Kalnay, 1993; Cai et al., 2003; Yang et al., 2006, 2008; Tang and Deng, 2010, 2011), the singular vector (SV) method (Farrell, 1989; Palmer et al., 1994) and the ensemble Kalman filter (EnKF) method (Evensen, 1994). All the initialization methods aim to satisify two conditions. One is to capture the uncertainties in the analysis; another is to grow the perturbation spanning the probable range of truth (Magnusson et al., 2008; Houtekamer and Derome, 1995).

The breeding method was previously used by the National Centers for Environmental Prediction (NCEP) until May 2006. This method is based on the idea that small but fast-growing perturbations saturate earlier (Yang et al., 2006). Therefore, by changing rescaling interval and rescaling amplitude, dominant perturbations of interest

can be isolated from faster growing perturbations which are no more than noise (Peña and Kalnay, 2004; Cai et al., 2003; Yang et al., 2006, 2008). Peña and Kalnay (2004) suggested that frequent rescaling of the order of 10 minutes can separate storm-scale signals. For larger-scale weather forecast, however, rescaling interval of 6 to 48 hours are recommended to create baroclinic initial perturbations. Cai et al. (2003) first showed that the BVs generated with 3 and 6-month rescaling intervals can successfully separate ENSO-related variabilities from weather and other shorter timescale variabilities. Yang et al. (2006, 2008) further asserted that rescaling period longer than two weeks can keep the slow, coupled instabilities in bred perturbations. However, few studies have been conducted concerning the effect of rescaling periods on prediction skill.

It is well known that there are a variety of time scales in tropical climate system (Kang and Kug, 2004; Lau and Weng 1999; Jin et al., 2003). In addition to 3-5 year ENSO cycle, near annual variability of 12-18 month period, decadal-interdecadal variability of more than 10-year period and even linear trend are superimposed on the tropical

phenomena. Therefore, it is important to take into consideration these various frequency modes to improve seasonal prediction skill over the tropical Pacific. Ham et al. (2012, in press) showed that BV1 (BV6) is driven by zonal advection feedback (thermocline feedback) and similar to high-frequency (typical ENSO) mode. Motivated by this result, the characteristics and the predictabilities of breeding methods with 3 different rescaling intervals (1, 3 and 6 months) are investigated in this study.

Along with BV, SV is another widely used initialization method. While breeding method keeps integrating model dynamics to filter out noisy modes, the singular vector method uses a mathematical technique to directly pick out optimal perturbations (Magnusson et al., 2008). The singular vector method performs singular value decomposition on a linear model using a linearized version of the dynamics to obtain a singular vector corresponding to the largest singular value. In this way, SV maximizes the growth over a fixed time interval and is consequently expected to dominate forecast errors (Buizza et al., 2005). The European Centre for Medium-Range Weather

Forecasts (ECMWF) has applied the singular vector method to weather forecast system. On a seasonal basis, however, SV method has some difficulties. Because this method requires a linearized version of a coupled model, it is problematic to capture variability associated with long-term timescale because the linearized system has a difficulty in capturing a nonlinear behavior when the lead time is long (Kug et al., 2010, 2011).

In an effort to apply the SV method to a nonlinear model, Kug et al. (2010) introduced empirical SV method. In ESV method, the operator (L) is estimated not by linearizing the governing equation but by using historical data from the long-term model integration. Kug et al. (2010, 2011) applied ESV method to both hybrid coupled model and sophisticated CGCM and showed the forecast skill for ENSO was improved. This study further investigates the effects of variables used to generate the empirical operator.

Based on the understanding of the characteristics of BVs and ESVs, the two methods are compared each other, and finally ensemble seasonal prediction skills are studied using SNU CGCM. There has

been several studies to compare the initialization methods (Buizza et al. 2005; Magnusson et al. 2008a,b; Bowler 2006; Smith et al. 1999; Trevisan et al. 1995; Anderson 1996). Nonetheless, many studies derived conclusions using simple models (Magnusson et al. 2008a,b; Bowler 2006; Smith et al. 1999; Trevisan et al. 1995; Anderson 1996) or not excluding different model effects (Buizza et al. 2005). Also, there have been few studies focusing on seasonal prediction.

The study is structured as follows. In section 2 the description of the model, data, initialization methods used and prediction experimental design are provided. The characteristics and prediction results of the breeding method and the empirical singular vector method are presented in section 3 and 4, respectively. The comparison of the methods and the ensemble results are explored in section 5, and conclusions are drawn in section 6.

2. Model and experimental design

2.1 SNU CGCM

The coupled GCM used in this study is SNU CGCM developed at Seoul National University. The oceanic part of the model is the Modular Ocean Model version 2.2 (MOM 2.2) developed at the Geophysical Fluid Dynamics Laboratory (GFDL). The ocean model uses a B-grid finite difference treatment of the primitive equations of motion, Boussinesq and hydrostatic approximations in spherical coordinates, and covers the global oceans with realistic coastlines and bathymetry. The zonal resolution is 1° and the meridional resolution is 1/3° between 8°S and 8°N, gradually increasing to 3° at 30°S and 30°N and fixed at 3° in the extratropics. There are 32 vertical levels with 23 levels in the upper 450 m with 10m thickness of the top 10 layers. A mixed layer model, developed by Noh and Kim (1999), is embedded into the ocean model to improve the climatological vertical structure of the upper ocean.

The atmospheric part of the SNU CGCM is SNU Atmospheric GCM (SNU AGCM). This is a global spectral model at T42 resolution, with 20 vertical sigma levels. The deep convection scheme is a

simplified Arakawa-Schubert scheme (Numaguti et al., 1995). The land surface model is from Bonan (1996), and the radiation process is parameterized by two-stream k-distribution scheme implemented by Nakajima et al. (1995). Other details of the model physics are described in Lee et al. (2001,2003).

The coupled model exchanges SST, wind stress, freshwater flux, longwave and shortwave radiation, and turbulent fluxes of sensible and latent heat.

The SNU CGCM well simulates the major ENSO phenomena such as an equatorial cold tongue along the equator over the eastern to central Pacific, even though some systematic biases exist (Ham et al., 2011).

2.2 Breeding method

Breeding methods is controlled by two parameters, the size of the initial perturbation amplitude (rescaling amplitude) and the length of

breeding interval (Cai et al., 2003). Bred vectors are known to be insensitive to the norm, which refers to the standard to calculate rescaling.

The breeding procedures are as follows:

Initially, both oceanic and atmospheric initial conditions are randomly perturbed and integrated for the rescaling period. Meanwhile an unperturbed initial conditions are also integrated. After a cycle of integration, the difference between the perturbed and the unperturbed runs are calculated and scaled down to maintain the initial amplitude of the chosen norm. Then, the rescaled perturbation is added to the initial condition of the unperturbed run for the next breeding cycle.

In this study, BVs are derived using three different rescaling intervals (1, 3 and 6 months) as mentioned before with the rescaling amplitude of 15%.

The decision of a rescaling amplitude is somewhat arbitrary. Although it is known that as the time scale of target phenomena gets longer, the rescaling amplitude gets larger, the rescaling amplitude

varies from 1% to 15% depending on the model and the rescaling norm used. For example, Vikhliaev et al. (2007) set the rescaling amplitude of 1%, while Cai et al. (2003) and Yang et al. (2006, 2008) used 10%, and Ham et al. (2012, in press) used 15% to capture ENSO mode. This study chose 15% following Ham et al. (2012, in press).

The norm is defined as the root mean square (RMS) of SST perturbation over the tropical Pacific region (120°E-90°W, 10°S-10°N) as belows:

$$\text{norm} = \sqrt{\frac{\iint_{\text{Pacific}} (\text{SST}_{\text{pert}} - \text{SST}_{\text{cntl}})^2 \text{dxdy}}{nx \cdot ny}} \qquad (1)$$

where nx, ny are the number of grids in x, y direction, and SST_{pert} , SST_{cntl} are monthly mean SST of perturbed run and control run, respectively.

The breeding procedure was repeated continuously for 20 years from January 1991 to December 2010. For the BV3 (BV6) to be generated every month, 3 sets (6 sets) of breeding were proceeded. For example, a breeding experiment of 3-month rescaling interval which started from January yields BVs only in January, April, July and October. Therefore, additional breeding experiments which start from

February and March are performed simultaneously to generate BVs for the entire months of a year.

2.3 Empirical singular vector method

The empirical singular vector method is basically same with the singular vector method, except that it uses an empirical linear operator. Both ESV and SV are based on the concept that the largest singular value of an operator (L) is an appropriate warning of uncertainties and its corresponding singular vector is an optimal initial perturbation for prediction.

In ESV, L is considered as a bridge between initial (X) and final (Y) state vectors as follows:

$$Y_n = X_{n+\tau} = LX_n + \varepsilon \qquad (2)$$

where n is time, τ is the lead time (optimization time) for model integration, and ε is the error from the linear approximation. If there are sufficient historical data from a model integration, the empirical linear operator can be written as

$$L=YX^t(XX^t)^{-1} \qquad (3)$$

This formula is the same as the linear inverse modeling approach (Blumenthal, 1991; Tziperman et al., 2008). By applying singular value decomposition (SVD) to L, the singular vectors can be calculated. When substitute the decomposed L to the equation (2),

$$u_i Y = s_i v_i X \qquad (4)$$

where u_i, v_i, and s_i are the i^{th} left, right singular vectors and singular value, respectively. When the singular value is greater than one, the corresponding right (left) singular vector is regarded as an initial (final) perturbation of growing mode.

In order to apply the ESV method to the prediction using the SNU CGCM, the linear operator is obtained in a reduced space through an empirical orthogonal function (EOF) analysis from the hindcast data of 1991-2010. The ENSO, target phenomenon of the seasonal prediction, is mostly explained by the thermocline feedback (Jin, 1997a). Therefore, for the initial state vector, X, the EOF analysis is applied to the thermocline depth data of the tropical Pacific (120°E-80°W, 20°S-20°N) from the initial condition of May. For the prediction state vector, Y, the EOF analysis is applied to the 6-month lead, which is November,

monthly mean SST data. The background knowledge about the choices of X and Y will be further discussed in section 4.

After applying EOF analysis to X and Y, only seven modes are used for constructing the operator. The seven EOF modes explain more than 81% and 93% of the total variance of the thermocline depth and the SST, respectively. With the principal components (PCs) of the seven EOF modes, the linear operator, L, is estimated.

From the linear operator, seven singular modes are extracted. Among these modes, singular vector whose corresponding singular value is the largest and above one is selected as the optimal perturbation.

In order to obtain the ESV patterns for the other variables in the model, the regressed patterns related to the EOF modes of the thermocline depth are constructed.

2.4 Seasonal prediction experiment

The hindcast experiments were conducted using the SNU CGCM. To obtain unperturbed initial conditions, a nudging method was

applied to the model for both the ocean and the atmosphere from January 1991 to December 2010. In the nudging method, a term that nudges a prognostic equation towards the observations is added to the solution. For example, the nudged temperature for the initial condition can be expressed as following equation.

$$\frac{\partial T}{\partial t} = -\bar{v} \cdot \nabla T + \frac{Q}{\rho C_p H} + \frac{T_{obs} - T}{\tau} \qquad (5)$$

The last term on the right hand side is the nudging term. T_{obs} refers to the observed temperature, and τ is the relaxation time scale.

In this study, ocean temperature and salinity data from NCEP Global Ocean Data Assimilation System (GODAS) reanalysis were used for nudging from surface to 500 m with 5-day relaxation time scale for the ocean. For the atmosphere, zonal and meridional wind, temperature, moisture and surface pressure from ERA-interim reanalysis of ECMWF were used for nudging for all vertical levels with 6-hour relaxation time scale.

Given the initial conditions, summer hindcast started in May with a 8-month leadtime every year from 1991 to 2010.

To verify the effects of the BV and ESV, LAF perturbations were

made with a 1-day lag generating 6 ensemble members in all (for more details on LAF, see Hoffmann and Kalnay, 1983).

Hereafter, the prediction with LAF perturbations is denoted as control prediction. The prediction with BV1, 3 and 6 are denoted as BV1, 3 and 6 prediction, respectively. Likewise, the prediction with ESV generated with thermocline depth and SST optimized at 6 month is denoted as ESV prediction.

3. The characteristics and prediction skills of BVs

In this section, the features and prediction skills of BVs upon different breeding intervals are explored. Figure 1 shows the 1st EOF modes of bred vector SST and thermocline depth from January 1991 to December 2010. The bred vector refers to the perturbation here. The 1st EOF SST patterns are almost identical in all BV cases (fig. 1a-c). The large amplitude signal in the eastern Pacific is a classical ENSO-like

structure (fig. 2a,b). In the case of thermocline depth, on the other hand, the location of maximum amplitude moves eastward as the integration time scale gets longer from 1 month to 6 months (fig. 1d-f). The maximum amplitudes in BV1, BV3, and BV6 thermocline depth variability appear approximately at 180°, 150°W, and 130°W, respectively. Also, the meridional distribution of BV1 thermocline depth EOF mode over the central to eastern Pacific is so narrow that doesn't exceed 5° from the equator, but becomes wider as the breeding interval gets longer. These results imply that the dynamics related to each BV might be different even though all the BVs successfully capture ENSO mode.

The EOF mode of BV6 thermocline depth depicts an east and west seesaw pattern, which means the thermocline is deepening (shoaling) in the eastern (western) Pacific. Both delayed oscillator model (Suarez and Schopf, 1988) and the recharge oscillator model (Jin, 1996, 1997a,b), which are the two prominent theories on ENSO dynamics, emphasize this kind of thermocline feedback. However, the observational evidence indicates that zonal advective process is also an important

mechanism for El Niño events (An and Jin, 2001; Kang et al., 2001). In this context, it is worth noticing that the 1st EOF mode of BV1 thermocline depth is more similar to the 2nd EOF mode than the 1st EOF mode of background thermocline depth (fig. 2c,d). This supports the hypothesis that BV1 and BV3 are driven by different dynamics with BV6. In this study, ocean reanalysis from GODAS for 20 years (1991-2010) was used as a background data. Ham et al. (2012, in press) also asserted that BV1 and BV6 are related with different mechanisms although they used different approaches to support their results.

To explore which kind of instabilities are reflected in the growths of BVs, the growth rates of the bred vectors are calculated based on the following equation:

$$G(t)=\frac{\sqrt{\sum_{\text{norm area}}[BV_{SST}(t)]^2}}{\sqrt{\sum_{\text{norm area}}[bv_{SST}(t-int)]^2}} \qquad (6)$$

where $BV_{SST}(t)$ is the SST difference between the perturbed run and unperturbed run at the end of breeding, namely time t, and $bv_{SST}(t-int)$ is the SST difference between the perturbed run and unperturbed run at the beginning of breeding, namely time t minus rescaling interval. This definition is similar to that in Yang et al. (2006).

Figure 3a shows the composite mean of the growth rate as a function of the background ENSO phase. The ENSO phases are categorized by the Nino3.4 index of background state and its tendency. It is summarized in Table 1. The red and grey areas in Fig. 3a refer to the El Niño peak and neutral periods, respectively. The growth rates of BV1 and BV3 have their peak when El niño is developing (bin number 3 and 4), and stay low during extreme El niño events (bin number 6 and 7). This result is consistent with that in Yang et al. (2006), Cai et al. (2003) and Tand and Deng (2011). The relationship between the BV growth rate and ENSO phase can be explained by a simple delayed oscillator model (Cai et al., 2003; Suarez and Schopf, 1988). According to the theory, upwelling Rossby waves induced by anomalous westerly propagate westward, and on reaching the western boundary, reflect into eastward propagating equatorial Kelvin waves. This reflected Rossby waves offset the downwelling Kelvin waves, lowering the SST over the eastern Pacific. This process can be written as,

$$\frac{dT}{dt} = T - T^3 - \alpha T(t - \delta) \qquad (7)$$

where, T represents the amplitude of the growing perturbation, t is time, δ is the delay time, and α is the influence of the delayed signal. If we assume T as control run solution, and $T + T^P$ as the perturbed run solution, (7) can be rewritten as a solution for the perturbation as follows (Cai et al. 2003):

$$\frac{dT^P}{dt} = (1 - 3T^2)T^P - \alpha T^P(t - \delta). \qquad (8)$$

Therefore, the perturbation T^P grows rapidly (slowly) when T is small (large), which is when background ENSO is in neutral (extreme) phase.

For BV6, on the other hand, this relationship between the BV growth rate and ENSO phase doesn't seem to work.

Figure 3b displays the composite mean of growth rate as a function of the calendar month. The month on the X-axis indicates the last month of breeding. The greatest growth rate appears when the breeding period goes through spring and summer in all three BV cases. For example, the growth rate of BV3 is high in September when the breeding proceeded from June to September. This kind of seasonal dependency corresponds with the findings of other studies (Cai et al.,

2003; Chen et al., 1997; Tang and Deng, 2011). The seasonal dependency shown in fig 3b is related to spring barrier in spring and strong baroclinic instability in summer. In their study on the ENSO's locking to the seasonal cycle, Tziperman et al. (1997) found that the most dominant factor is the wind divergence field, as determined by the seasonal motion of the Pacific intertropical convergence zone (ITCZ). They also concluded that the next-order seasonal effect is due to the seasonality of the background SST and ocean upwelling velocity. ITCZ is the closest from the equator in spring, thereby enhancing convective instability. During summer, large mean SST gradients and strong mean upwelling increase the coupling strength between the ocean and atmosphere, which lead to strong baroclinic instability (Xue et al. 1997a).

Unlike BV3 and BV6, BV1 has one more peak in early winter. It is known that tropical instability waves (TIW) are active when cold tongue is apparent, which coincides with boreal fall (Yang et al., 2006). This implies that BV1 is more affected by high frequency modes than BV3 and BV6. The fact that the monthly mean growth rates gradually

decrease (not shown) from 1.8/mon (BV1) to 0.9/mon (BV3) to 0.5/mon (BV6) also supports this idea.

Figure 4 shows the composite perturbation on May of El niño and La niña years. Because the hindcast experiments started from May, this figure implies how the perturbation would evolve when prediction starts. The SST perturbation of BV3 has a warm perturbation along the cold tongue area in El niño years (fig. 4b). For the other cases, the warm perturbations are either concentrated in the eastern Pacific (fig. 4a) or too vague (fig. 4c). Similar conclusions can be drawn with subsurface temperature initial perturbation (fig. 4d-4f). The temperature perturbation in the subsurface reflects deepening (shoaling) perturbation of thermocline in the eastern (western) Pacific, which is an classical ENSO feature. Like El niño years, cold SST perturbation over cold tongue area during La niña years is well captured by BV3 (fig. 4h), while it is clustered in the far-eastern Pacific in BV1 case (fig. 4g). It is interesting that BV6 shows warm perturbation in La niña years (fig. 4i). This can be interpreted that during the 6 months of breeding, the tendency changes, so that BV6

fails to isolate La Niña-related signal.

So far the characteristics of BVs of different rescaling intervals were investigated, and BV3 turns out to be the most favorable for ENSO prediction. To verify this idea, the predictabilities are tested. Figure 5 shows the correlation coefficients of 3 kinds of nino indices as a function of forecast lead month. The correlation skill of BVs is higher or similar to that of LAF. Considering that the number of LAF ensemble members is 3 times more than that of each BV prediction, the breeding method is an efficient way to raise predictability with fewer ensemble members. Among three kinds of BV predictions, BV3 showed the highest forecast skill for nino 3.4 and nino 4 indices regardless of forecast lead month. This result is supported by initial perturbation pattern shown in fig 4a-4c, 4g-4i.

Between BV1 and BV6, the regional dependency of predictability is clear. In the western Pacific, the overall predictability represented by nino 4 index is higher in BV1 prediction than in BV6 prediction. However, in the eastern Pacific, the run with BV6 is superior to both BV1 and BV3. It is known that different mechanisms induce

anomalous warming over Nino 4 and 3 areas. While vertical advection is a key process to the development of SST anomalies in the Nino-3 region, zonal advection plays a crucial role in the SST evolution in the Nino-4 region (Kug et al., 2009, 2010; Ashok et al., 2007). Ham et al. (2012, in press) showed that zonal advective (thermocline) feedback is a crucial mechanism for generating BV1 (BV6) SST using the SNU CGCM. Therefore, BV1 excels in Nino-4 prediction, and BV6 is superior in Nino-3 prediction. Over Nino-3.4 region, the correlation skills of BV1 and BV6 predictions were similar. However, when the results of BV1 and BV6 predictions were ensemble averaged, the correlation skill of Nino-3.4 index was improved by 0.047 and 0.031, on average, after lead month 2 compared to the single forecasts of BV1 and BV6 prediction, respectively (not shown). Also, the predictability of ensemble results was similar to the single forecasts of BV3 prediction. This means that a pair of BV3 is an optimal perturbation whose prediction skill is comparable to the 4 ensemble members from BV1 and BV6 predictions (not shown).

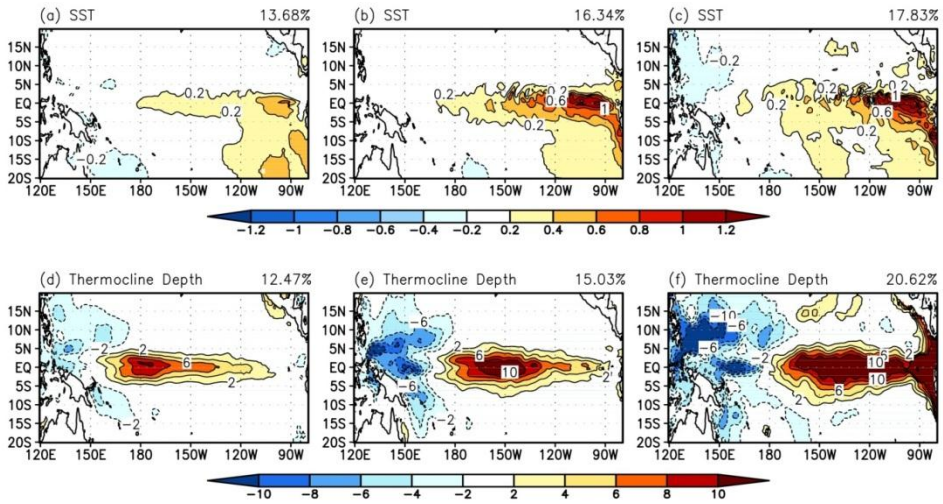

Figure 1. 1st EOF mode of bred vector SST (upper panel) and thermocline depth (lower panel)

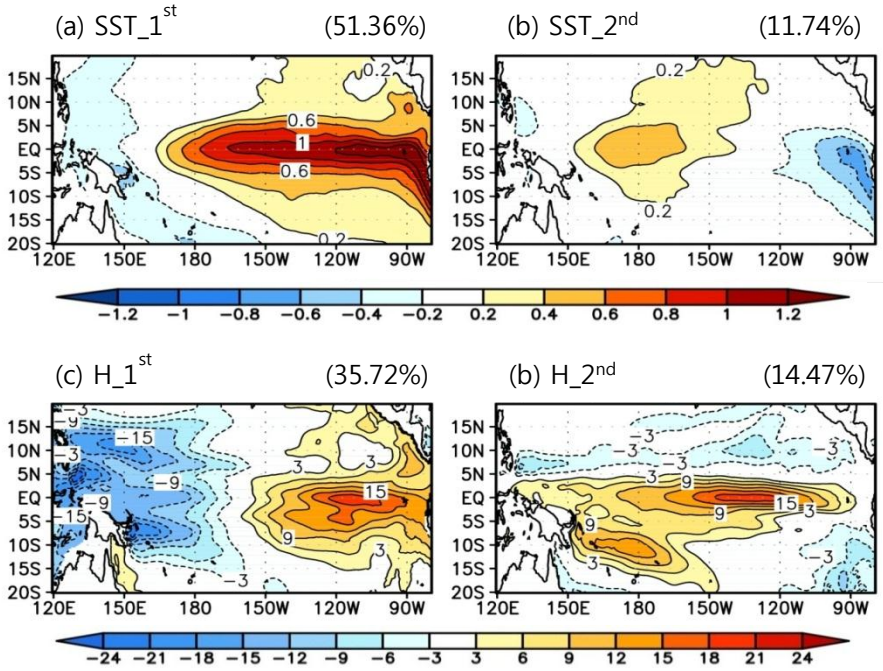

Figure 2. 1st EOF mode of observed SST (upper panel) and thermocline depth (lower panel)

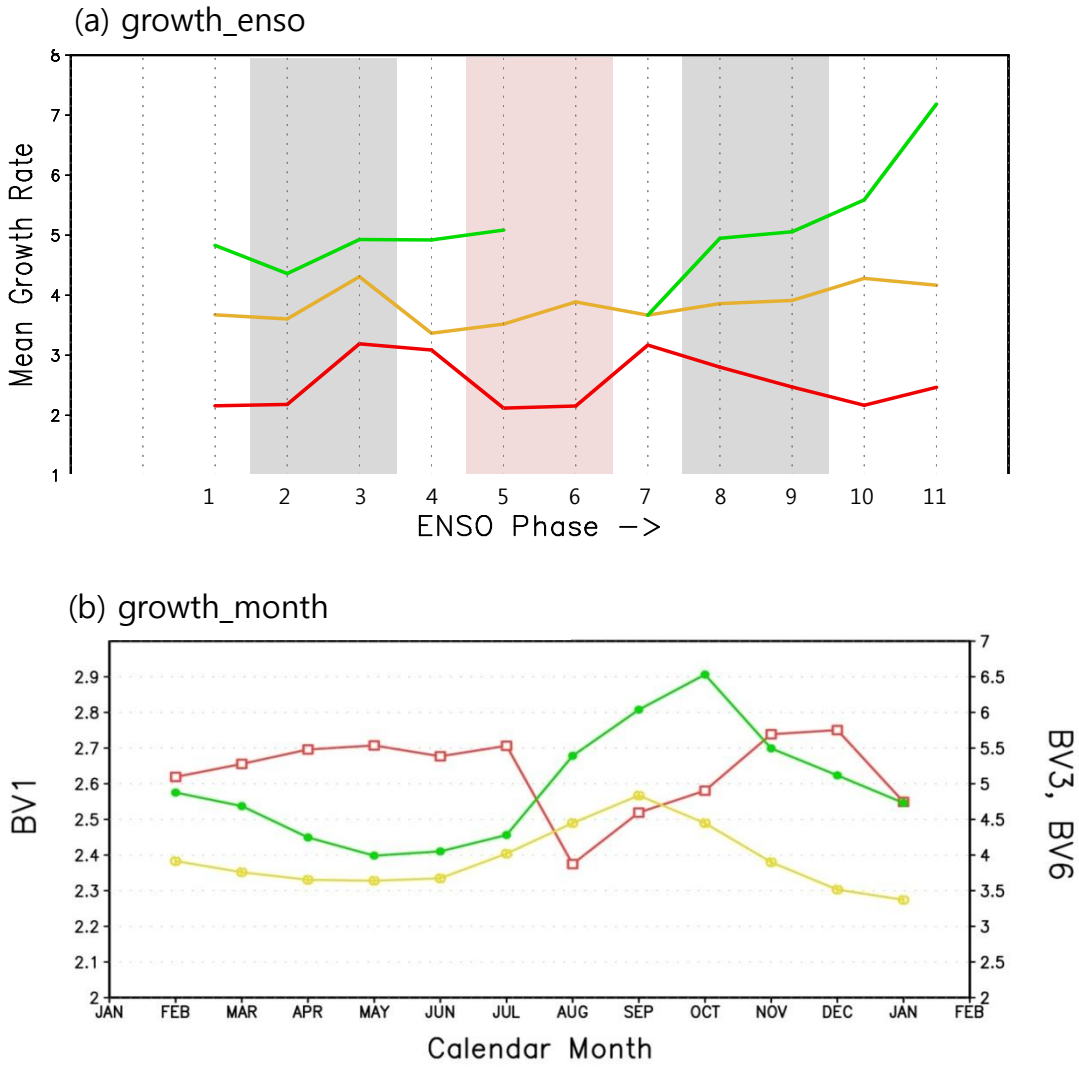

Figure 3. (a) Growth rates of BV1 (red line), BV3 (yellow), BV6 (green) as a function of ENSO phase. (b) as in (a) but as a function of calendar months. The month indicates the last month of breeding.

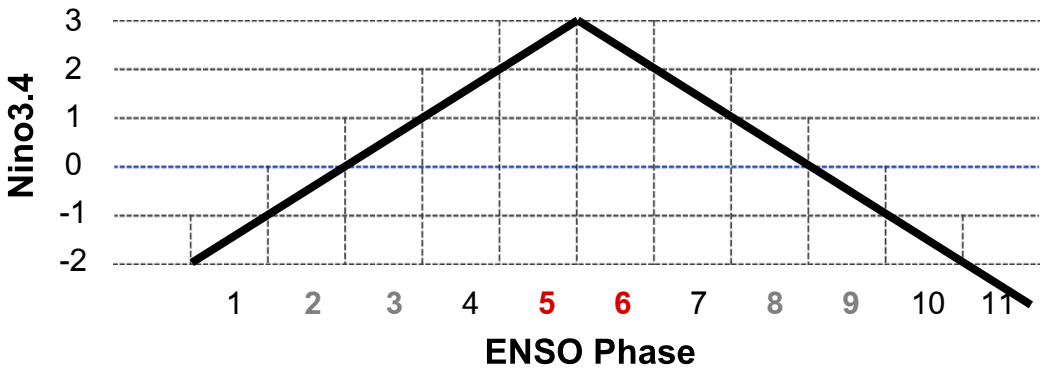

	Bin number										
	1	2	3	4	5	6	7	8	9	10	11
lower	-2	-1	0	1	2	2	1	0	-1	-2	-3
upper	-1	0	1	2	3	3	2	1	0	-1	-2
tendency	+	+	+	+	+	-	-	-	-	-	-

Table 1. The ENSO phases categorized by the Nino3.4 Index of background state and its tendency

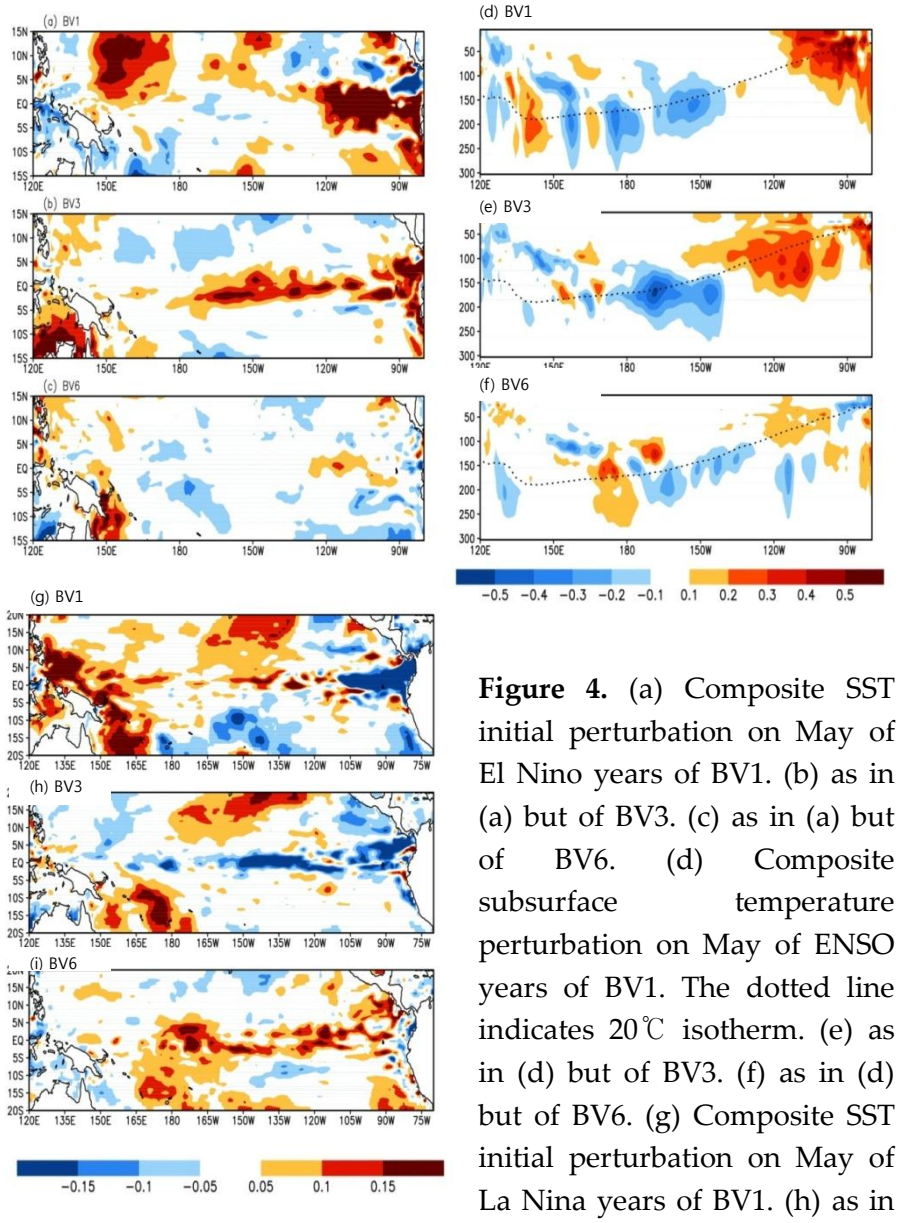

Figure 4. (a) Composite SST initial perturbation on May of El Nino years of BV1. (b) as in (a) but of BV3. (c) as in (a) but of BV6. (d) Composite subsurface temperature perturbation on May of ENSO years of BV1. The dotted line indicates 20℃ isotherm. (e) as in (d) but of BV3. (f) as in (d) but of BV6. (g) Composite SST initial perturbation on May of La Nina years of BV1. (h) as in (g) but of BV3. (i) as in (g) but of BV1. The El Nino years are 1991, 94, 97, 02, 06 and 09. The La Nina years are 1995, 98, 99, 07, 10.

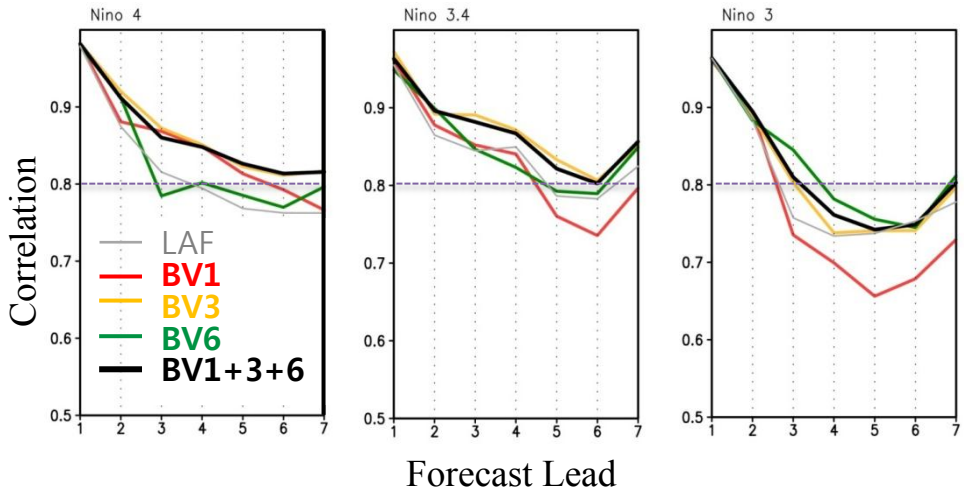

Figure 5. Correlation skill of three kinds of Nino indices (Nino4, Nino3.4 and Nino3) of LAF (grey), BV1 (red), BV3 (yellow), BV6 (green), ensemble mean of all BVs (BV1+3+6, black)

4. The characteristics and prediction skills of ESVs

As previously mentioned, the empirical linear operator (L) in the equation (2) and (3) is constructed using initial state vector (X) and final state vector (Y) with a certain time interval between them. Therefore, prior to analyze the prediction skills of ESV, the effects of state vectors and optimization time (the interval that the final state vector leads the initial state vector) are investigated.

As in Kang et al. (2001), the SST equation in the equatorial Pacific can be written as

$$\frac{\partial T'}{\partial t} = -u' \frac{\partial \overline{T}}{\partial x} - \frac{\partial (\overline{v} T')}{\partial x} - \overline{w} \frac{\partial T'}{\partial z} - Q' \qquad (9)$$

where T′ is the SST anomaly, u′ is the anomalous zonal currents, Q′ is other residual terms. Considering that the second term on the right hand side can be effectively included in the Newtonian cooling term, the SST in the equatorial Pacific is mostly controlled by two terms: the zonal advection of mean SST by anomalous current, and the vertical advection of anomalous subsurface temperature by the mean

upwelling. On the assumption that the zonal current anomaly and thermocline depth anomaly are the measures of zonal and vertical advection, the lag correlations of Nino-3.4 index with zonal current anomaly and thermocline depth anomaly are obtained using reanalysis data(fig 6). The numbers written on the left of left panel refer to the months by which the variables (zonal current and thermocline depth) leads the Nino-3.4 index. Although the correlation coefficients of Nino-3.4 index with zonal currents are smaller than that with thermocline depth, the zonal current shows meaningful relationship with SST several months before El Niño event reaches its peak. Thermocline depth has stronger relationship with SST. It shows a correlation above 0.4 even 10 months prior to the time when ENSO amplitude reaches its maximum.

Based on this, the EOF analysis was applied to the zonal current and the thermocline depth data from the initial condition of May for the initial state vector X. For the prediction state vector, Y, the EOF analysis is applied to monthly mean SST data with different lead time. The lead time was set to 1 month when zonal current data were used

for X, while it was set to 3 and 6 months when thermocline depth data were used. This is because it is plausible to think that the ocean memory for ENSO provided by vertical advection is longer than that by zonal advection. The ESVs generated with zonal current (thermocline depth) and SST with 1 month (3 months; 6 months) lead time is denoted as U01 (H03; H06).

Figure 7a shows the singular values of U01, H03 and H06. It is seen that all cases contain singular values greater than 1. In U01, the 1st singular value is 2.71, and the 2nd and 3rd singular values also exceed 1. This means that there exist three kinds of growing modes, therefore it may not enough to use one singular vector. In case of H03, the largest singular value is not distinctively isolated from smaller singular values, either. The 1st and the 2nd singular values of H03 is 2.05 and 1.01, respectively. On the other hand, H06 has the 1st singular values well separated from the other singular values.

It is clear that the characteristics of the singular values have influences to prediction results, as shown in fig 7b. The correlation skills of Nino-3.4 index is the highest in the prediction with H06. The

predictions with U01 and H03 are less skillful than those with H06. Especially, the correlation coefficients of the run with H03 are lower than those of LAF prediction shown in fig 5. These results indicate that ESV is sensitive to the choices of the state variables and optimization time. Therefore, in order for the ESVs to improve predictability, the 1st singular values should be greater than 1 and distinguished from smaller singular values, so that one dominant growing mode is captured. Hereafter, the prediction with H06 is denoted as ESV prediction.

Figure 8 shows the first leading singular mode obtained with the ESV method (H06). The initial state of thermocline depth in fig. 8a exhibits the pattern of ENSO developing phase described in Jin (1997). After 6 months, the SST field shows east and west dipole pattern in fig. 8b. These features are consistent with the singular modes of Xue et al. (1997). Using the initial conditions generated with the initial perturbation shown in fig 8a, seasonal prediction from 1991-2010 is performed. It is noteworthy that the same perturbation was added to and subtracted from unperturbed background every year.

Figure 9 shows the correlation skill of three nino indices as a function of forecast lead month. The forecast skill of ESV prediction with two ensemble members is remarkably higher than that of LAF prediction with six ensemble members. The forecast skill improvement is distinctive for long lead months. The correlation coefficients of Nino-3.4 and 4 index record approximately 0.9 at lead month 7.

One may wonder why the ESV method leads to such a good prediction skill even though the same perturbation was used every year. It will probably be because background state plays an crucial role in the growth of perturbation. In other words, the same perturbation can grow variously depending on the background state such as El-Nino or La-Nina.

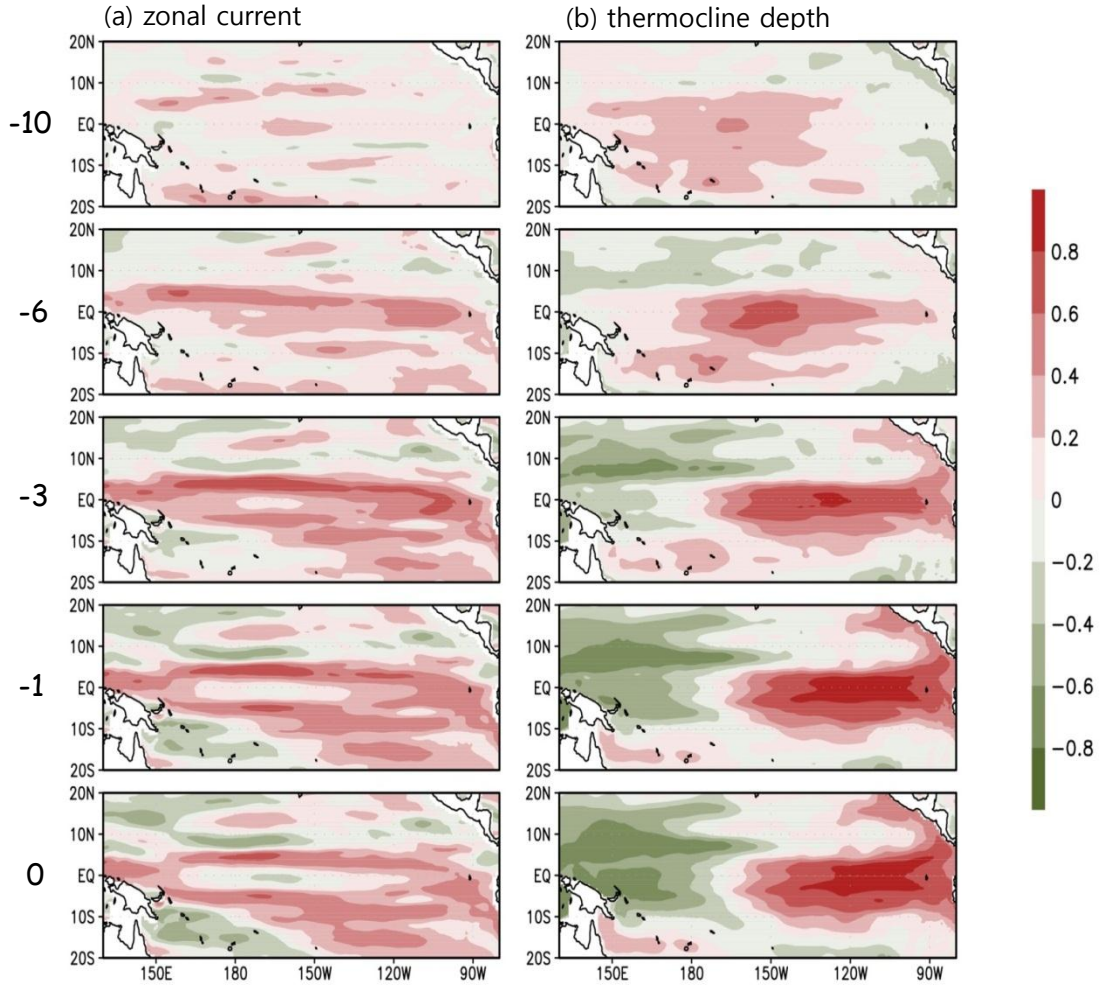

Figure 6. The lag correlation of Nino 3.4 index with zonal current anomaly (left panel) and thermocline depth anomaly (right panel). The numbers written on the left of left panel indicate the month by which zonal current and thermocline depth leads the nino 3.4 index

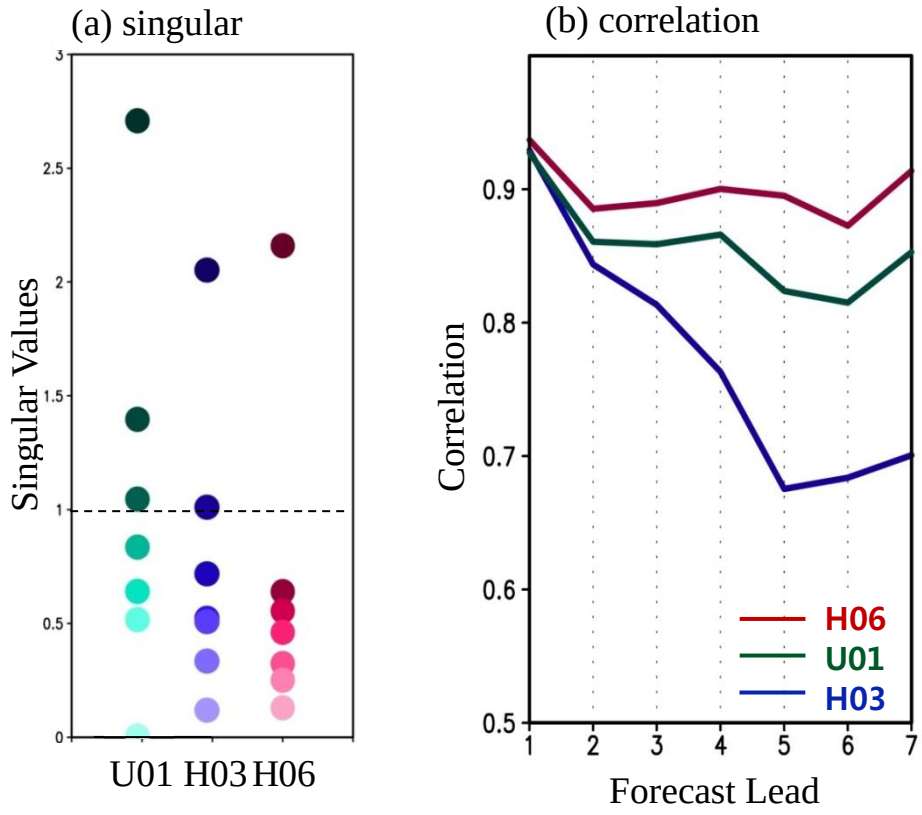

Figure 7. (a) Singular values of ESV experiments. The alphabets in U01, H03, H06 stand for variables of initial state. U is zonal current, and H is thermocline depth. For the variable of final state, SST was used in all experiments. The numbers is the time intervals between initial and final variables. (b) correlation coefficients of each ESV predictions.

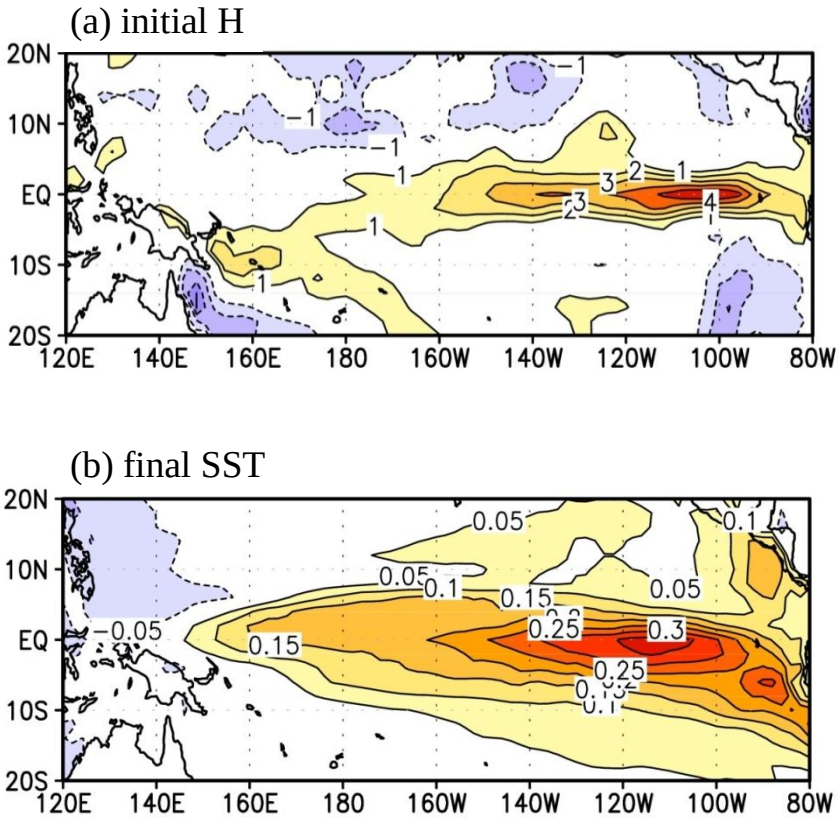

Figure 8. 1st leading singular mode of (a) thermocline depth in May, and (b) SST.

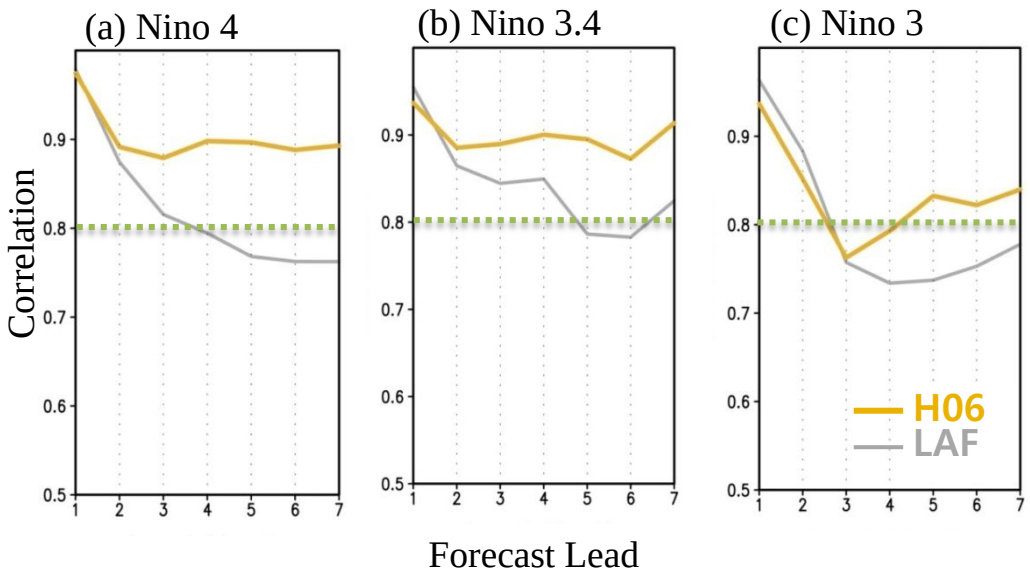

Figure 9. Correlation skill of three kinds of Nino indices (Nino4, Nino3.4 and Nino3) of LAF (grey), ESV (yellow) prediction

5. Results of ensemble mean

To compare the results of BV and ESV predictions and to assess the prediction skill of ensemble mean composed of both predictions, correlation coefficient and root mean square error (RMSE) are calculated in figs 10. Note that the predictions with BV3 and H06 which showed the best prediction skill in each perturbation method are used for the calculation of correlation and RMSE. The results suggest that breeding method is marginally better than ESV method for short lead times. BV predictions show higher correlation and lower RMSE until 2-3 lead months. As the lead time gets longer, however, ESV method outperforms breeding method. The correlation coefficient and the RMSE of ESV prediction is 0.1 higher and 0.16 lower, respectively, compared to those of BV3 prediction. The ensemble prediction for two perturbation strategies, breeding and empirical singular vector methods, appears to be following better strategy between the two. After the ensemble averaging, the correlation remains stably high but, there is no significant correlation difference

before and after the ensemble avaraging. There are possibilities that BV3 and ESV picked up dynamically identical mode, thereby providing limited error reduction effect.

The global correlation maps for SST are also consistent with these results as shown in figs 11a-i. At the beginning the correlation skill of BV prediction is higher not only in the tropics but also in the extratropics (fig. 11b,c). However, at lead month 5, the overall correlation skill is higher in ESV prediction than in BV3 prediction (fig. 11h,i). When ensemble averaged, the spatial distribution of correlation resembles that of BV3 prediction at the beginning, but becomes more similar to that of ESV prediction (fig. 11g-i).

This study does not necessarily insist that one method is superior to another. It must be kept in mind that the performance of perturbation methods strongly depends on the numerical model used to generate predictions (Wei and Toth, 2003; Buizza et al., 2005). In their study on the ensemble forecast skill, Wei and Toth (2003) showed that when perturbations were used to explain errors made with the other center's model, their skill was dramatically reduced at long lead

times.

Nonetheless, it is worth noticing that many recent studies on the comparison of initialization methods suggest that error breeding is superior to singular vector method for short lead times, while the singular vector method becomes superior or at least similar to breeding method as the prediction continues (Wei and Toth, 2003; Buizza et al., 2005). For example, Wei and Toth (2003) showed that the NCEP (ECMWF) ensemble generated by breeding method (singular vector method) has better performance before (after) 3-day lead time over the tropics. Bowler (2006) pointed out that the breeding ensemble is worse than other methods in terms of the spread versus RMSE.

Figure 12 shows the spread to error ratio. The ratio is calculated according to the following equation:

$$\text{spread to error ratio} = \frac{\frac{1}{Nm}\sum_{j=1}^{N}\sum_{i=1}^{m}(X_{ij}-\overline{x_j})^2}{\frac{1}{N}\sum_{j=1}^{N}(\overline{X_j}-O_j)^2} \qquad (10)$$

The subscript i is individual ensemble member, j is individual year, and N and m are the number of hindcast years (20 years in all cases) and the number of emsemble members. X and O indicate prediction result and observation value, respectively.

Initially the ratio of the breeding method is 2-4 times greater than LAF method, the control run (fig 12a). However, the ratio of control prediction outgrows that of BV prediction after lead month 2-3. This is mostly because the spread of BV prediction doesn't increase fast enough (not shown). In comparison, the spread to error ratio of ESV prediction is greater than that of control prediction regardless of lead month and region. The ratio decreased by 0.22, on average, after BV3 and ESV predictions are ensemble averaged, due to the small ensemble spread in BV3 prediction.

To provide further insight into the prediction skills, signal to noise (STN) ratio is introduced. It was calculated upon SST. The STN ratio is defined as (Kang and Shukla, 2006)

$$\text{STN ratio} = \frac{\sigma^2_{\text{signal}}}{\sigma^2_{\text{noise}}} \qquad (11)$$

$$\sigma^2_{\text{signal}} = \frac{1}{N-1}\sum_{j=1}^{N}\left(\overline{x_j} - \overline{\overline{x}}\right)^2$$

$$\sigma^2_{\text{noise}} = \frac{1}{N(m-1)}\sum_{j=1}^{N}\sum_{i=1}^{m}(x_{ij} - \overline{x_j})^2.$$

Notations are the same as in equation (10), with $\bar{\bar{x}}$ refers to the climatological mean of ensemble mean. The signal is considered as the

external component forced by explicit SST forcing, while the noise is related to the stochastic internal component such as the atmospheric nonlinear dynamics. When STN ratio is larger, the SST is less controlled by the noise and thus more predictable.

Figure 13 shows the relationship between the STN ratio and correlation improvement over control prediction in Nino-3.4 region at lead month 3. In BV3 prediction, the correlation improved where the region is predictable (fig. 13a). In the ESV and the ensemble prediction, the correlation improvement was clear over the unpredictable region (fig. 13b,c). Especially, in the ensemble prediction, the correlation improvement is inversely proportional to the STN ratio (fig. 13c). This means the ensemble averaging worked more effectively where the forecast skill is sensitive to the uncertainty of the initial condition.

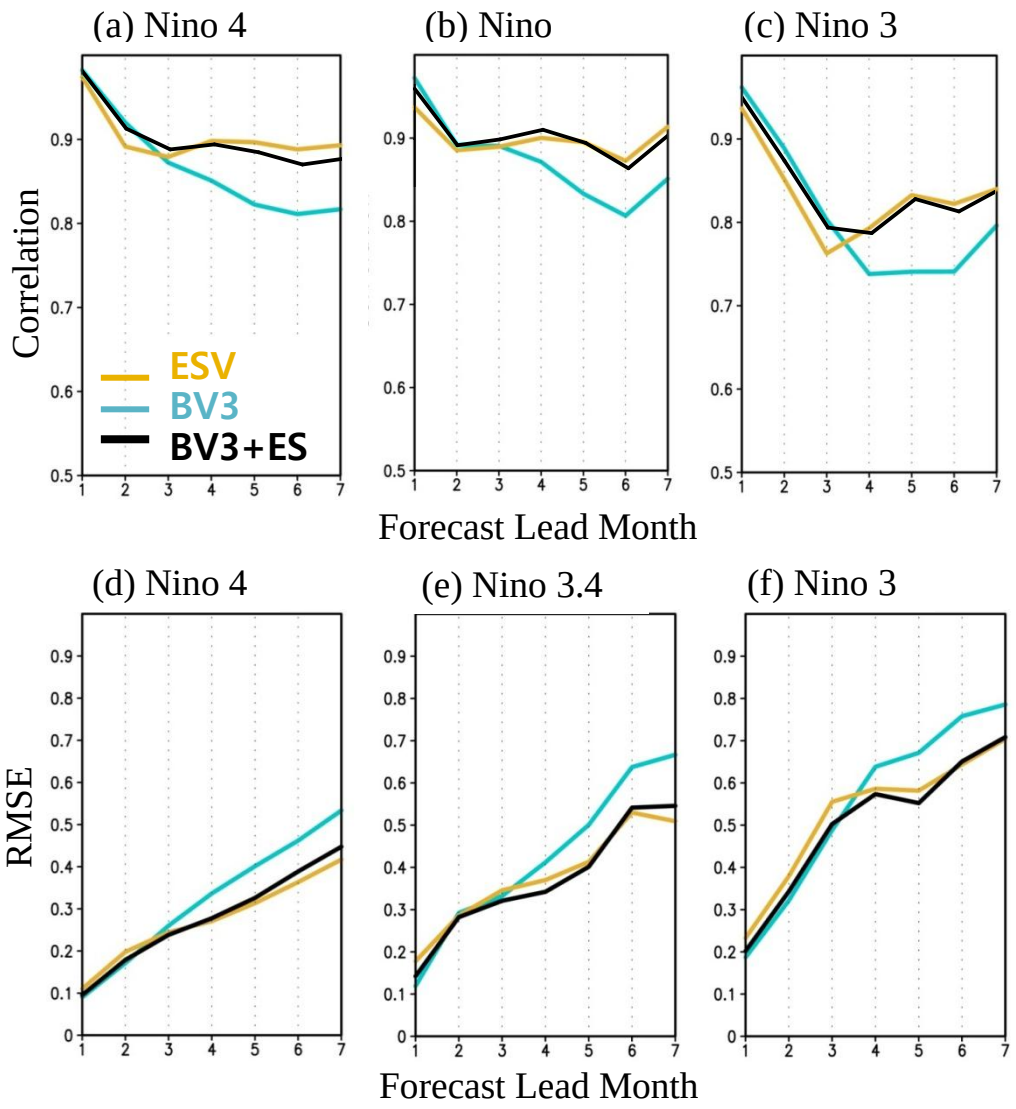

Figure 10. (upper) Correlation skill of three kinds of Nino indices (Nino4, Nino3.4 and Nino3) of ESV (yellow), BV3 (blue), and ensemble of BV3 and ESV (black) predictiton. (lower) as in (top) but for RMSE

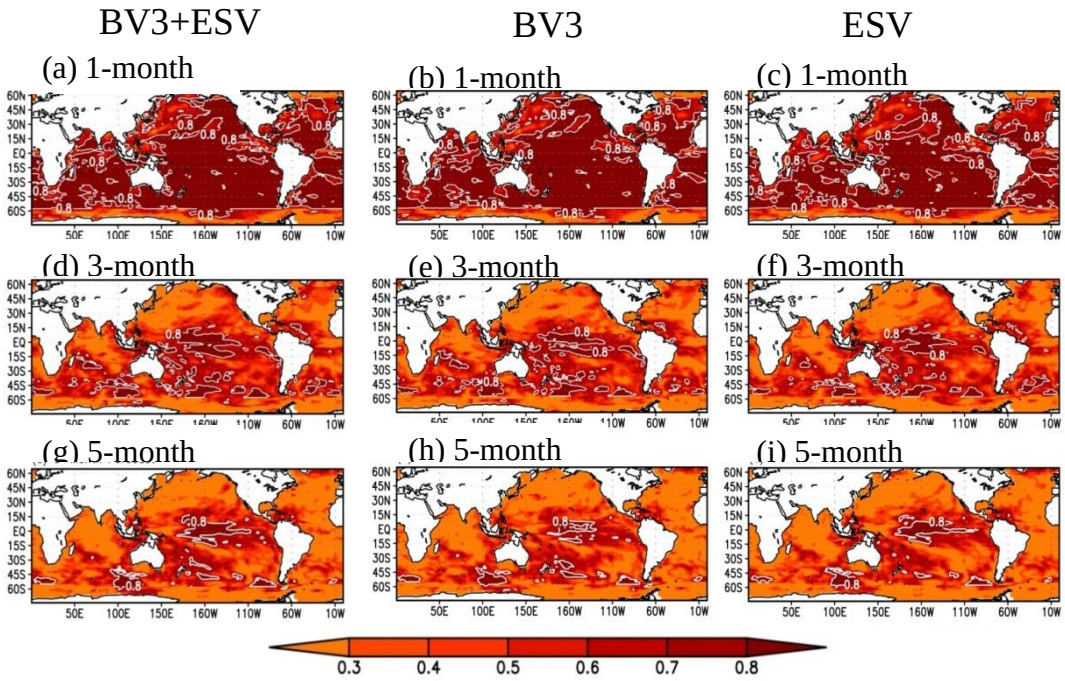

Figure 11. Correlation skill of SST in ensemble (left), BV3 (middle), and ESV (right) prediction. The months written on the maps refer to the forecast lead month

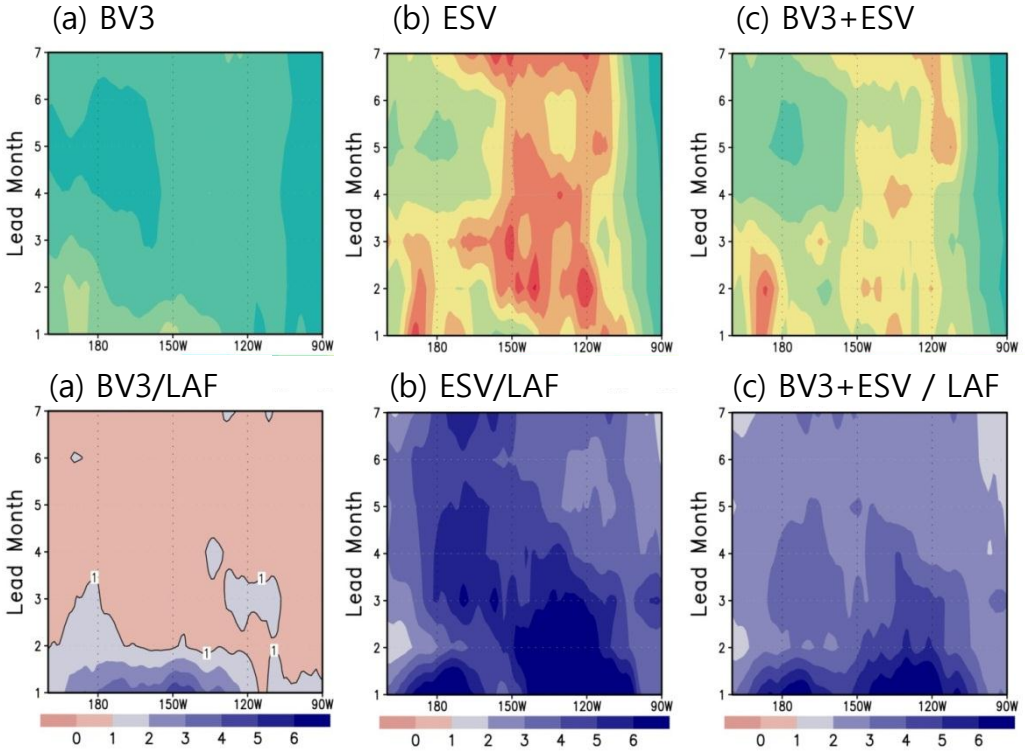

Figure 12. (upper panel) Ensemble spread to error ratio of (a) BV3, (b) ESV and (c) ensemble of BV3 and ESV. (lower panel) ensemble spread to error ratio of BV3, ESV and ensemble prediction divided by that of control prediction.

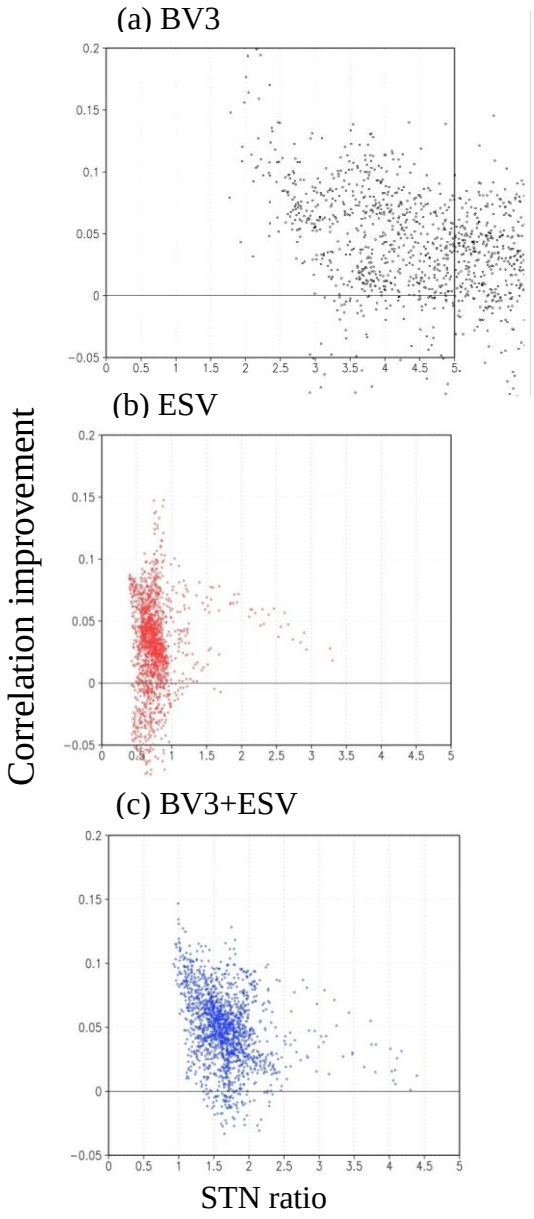

Figure 13. Scatter diagram between STN ratio (x-axis) and correlation improvement (y-axis) over nino3.4 area at lead month 3

6. Summary and Discussions

This study focused on the ensemble prediction generated with different initialization methods and the comparison of the methods using the SNU CGCM. Six initial perturbations were generated by the breeding method with three different breeding intervals of 1, 3 and 6 months. With ESV method, a pair of perturbations was constructed based on thermocline depth and SST. For control experiment, 6 initial perturbations were generated with LAF method. Hindcasts were carried out for the period of 20 years (from May 1, 1991-2010).

In BV experiment, all kinds of BVs captured ENSO mode, and the prediction skills with them were superior to LAF predictions. Especially the correlation skills of Nino3.4 and Nino 4 indices of BV3 prediction were comparable to that of ensemble prediction of BV1, 3 and 6. The ESV was sensitive to the initial state variable and the optimization time. In order for the ESV to be an optimal perturbation, the 1st singular value should be greater than 1 and well distinguished from smaller singular values. In SNU CGCM system, the prediction

skill was as high as 0.9 at lead month 7 when the initial state variable and the optimization time were set to thermocline depth and 6 month, respectively. The predictions with ESV perturbations showed better performances after 2-3 lead months than those with BV3 perturbations. When the predictions of BV3 and ESV were ensemble averaged, the predictability dependency on lead time decreased, but no significant correlation improvement was shown compared to the BV3 or the ESV prediction. The spread to error ratio of BV3 prediction was greater than that of control prediction only for short lead times, while the ratio of the ESV prediction was 2-6 times larger than that of LAF prediction regardless of forecast lead months. In addition, the correlation skill improvement of BV3 (ESV) prediction was distinct in predictable (unpredictable) region. After the ensemble averaging of BV3 and ESV predictions, the more the region is affected by noise, the more the correlation was improved.

This was one of the few studies to compare perturbation methods and to assess ensemble averaging impact under the same full coupled model environment. The results confirmed that the seasonal prediction

skill can be greatly improved using not more than 4 ensemble members generated by breeding and empirical methods.

However, it should be kept in mind that the results are dependent on models, and thus are not necessarily applied to other models. Also, in addition to correlation skill, spread to error ratio and STN ratio, more elaborate measures are needed to corroborate these results.

Despite these constraints, this study will be able to provide information about the characteristics of BVs and ESVs, and the impact of ensemble averaging in a broad sense. The understanding of perturbation methods, in turn, will suggest ways to improve predictability of not only classical El Niño event but also different types of events such as warm pool El Nino.

Acknowledgements

This work was supported by the National Research Foundation of Korea (NRF) grant funded by the Korean government (MEST) (NRF-

2009-C1AAA001-2009-0093042). This work was also supported by the Brain Korea 21 Project in 2012.

Reference

An, S. I. and F. F. Jin (2001). "Collective role of thermocline and zonal advective feedbacks in the ENSO mode*." Journal of climate 14(16): 3421-3432.

Anderson, J. L. (1996). "Selection of initial conditions for ensemble forecasts in a simple perfect model framework." Journal of the atmospheric sciences 53(1): 22-36.

Ashok, K., S. K. Behera, et al. (2007). "El Niño Modoki and its possible teleconnection." J. Geophys. Res 112(10.1029).

Benno Blumenthal, M. (1991). "Predictability of a coupled ocean-atmosphere model." Journal of climate 4: 766-784.

Bonan, G. B. (1996). Land surface model (LSM version 1.0) for ecological, hydrological, and atmospheric studies: Technical description and users guide. Technical note, National Center for Atmospheric Research, Boulder, CO (United States). Climate and Global Dynamics Div.

Bowler, N. E. (2006). "Comparison of error breeding, singular vectors, random perturbations and ensemble Kalman filter perturbation strategies on a simple model." Tellus A 58(5): 538-548.

Buizza, R., P. Houtekamer, et al. (2005). "A comparison of the ECMWF, MSC, and NCEP global ensemble prediction systems." Monthly Weather Review 133(5): 1076-1097.

Cai, M., E. Kalnay, et al. (2003). "Bred vectors of the Zebiak-Cane

model and their potential application to ENSO predictions." Journal of climate 16(1): 40-56.

Chen, Y. Q., D. S. Battisti, et al. (1997). "A Study of the Predictability of Tropical Pacific SST in a Coupled Atmosphere-Ocean Model Using Singular Vector Analysis: The Role of the Annual Cycle and the ENSO Cycle*." Monthly Weather Review 125(5): 831-845.

Evensen, G. (1994). "Sequential data assimilation with a nonlinear quasi-geostrophic model using Monte Carlo methods to forecast error statistics." JOURNAL OF GEOPHYSICAL RESEARCH-ALL SERIES- 99: 10-10.

FARRELL, B. (1989). "Optimal excitation of baroclinic waves." Journal of the atmospheric sciences 46(9): 1193-1206.

Ham, Y. G., I. S. Kang, et al, (2011). "El-Nino Southern Oscillation simulated and predicted in SNU coupled GCMs" Climate Dynamics doi:10.1007/s00382-011-1171-5

Ham, Y. G., I. S. Kang, et al. (2012). "Coupled Bred Vectors in the Tropical Pacific and Their Application to ENSO Prediction." Progress In Oceanography.

Hoffman, R. N. and E. Kalnay (1983). "Lagged average forecasting, an alternative to Monte Carlo forecasting." Tellus A 35(2): 100-118.

Houtekamer, P. and J. Derome (1995). "Methods for ensemble prediction." Monthly Weather Review 123(7): 2181-2196.

Jin, F. F. (1996). "Tropical ocean-atmosphere interaction, the Pacific cold tongue, and the El Niño-Southern Oscillation." Science 274(5284):

76-78.

Jin, F. F. (1997a). "An equatorial ocean recharge paradigm for ENSO. Part I: Conceptual model." Journal of the atmospheric sciences 54(7): 811-829.

Jin, F. F. (1997b). "An equatorial ocean recharge paradigm for ENSO. Part II: A Stripped-Down Coupled Model." Journal of the atmospheric sciences 54(7): 830-847.

Jin, F. F., J. S. Kug, et al. (2003). "A near-annual coupled ocean-atmosphere mode in the equatorial Pacific ocean." Geophysical research letters 30(2): 1080.

Kang, I. S., S. I. An, et al. (2001). "A systematic approximation of the SST anomaly equation for ENSO." 気象集誌 79(1): 1-10.

Kang, I. S., J. S. Kug, et al. (2004). "A near-annual Pacific Ocean basin mode." Journal of climate 17(12): 2478-2488.

Kang, I. S. and J. Shukla (2006). "Dynamic seasonal prediction and predictability of the monsoon." The Asian Monsoon: 585-612.

Kug, J. S., J. Choi, et al. (2010a). "Warm pool and cold tongue El Nino events as simulated by the GFDL 2.1 coupled GCM." Journal of climate 23(5): 1226-1239.

Kug, J. S., Y. G. Ham, et al. (2010b). "New approach for optimal perturbation method in ensemble climate prediction with empirical singular vector." Climate dynamics 35(2): 331-340.

Kug, J. S., Y. G. Ham, et al. (2011) "Empirical Singular Vector (ESV) Method for Ensemble ENSO Prediction with a Coupled GCM." J.

Geophys. Res., 116

Kug, J. S., F. F. Jin, et al. (2009). "Two types of El Niño events: cold tongue El Niño and warm pool El Niño." Journal of climate 22(6): 1499-1515.

Lau, K. and H. Weng (1999). "Interannual, decadal-interdecadal, and global warming signals in sea surface temperature during 1955-97." Journal of climate 12(5): 1257-1267.

Lee, M. I., I. S. Kang, et al. (2001). "Influence of cloud-radiation interaction on simulating tropical intraseasonal oscillation with an atmospheric general circulation model." Journal of geophysical research 106(14): 219-214

Lee[1], M. I., I. S. Kang, et al. (2003). "Impacts of cumulus convection parameterization on aqua-planet AGCM simulations of tropical intraseasonal variability." 気象集誌 81(5): 963-992.

Magnusson, L., E. Källén, et al. (2008). "Initial state perturbations in ensemble forecasting." Nonlinear Processes Geophy 15: 751-759.

Magnusson, L., M. Leutbecher, et al. (2008). "Comparison between singular vectors and breeding vectors as initial perturbations for the ECMWF ensemble prediction system." Monthly Weather Review 136(11): 4092-4104.

Nakajima, T., M. Tsukamoto, et al. (1995). "Modelling of the radiative processes in an AGCM." Climate system dynamics and modelling 3: 104-123.

Noh, Y. and H. J. Kim (1999). "Simulations of temperature and

turbulence structure of the oceanic boundary layer with the improved near-surface process." Journal of geophysical research 104: 15.

Numaguti, A., M. Takahashi, et al. (1995). "Development of an atmospheric general circulation model." Climate system dynamics and modelling 3: 1-27.

Palmer, T., R. Buizza, et al. (1994). "Singular vectors and the predictability of weather and climate." Philosophical Transactions of the Royal Society of London. Series A: Physical and Engineering Sciences 348(1688): 459-475.

Peña, M. and E. Kalnay (2004). "Separating fast and slow modes in coupled chaotic systems." Nonlinear Processes in Geophysics 11(3): 319-327.

Smith, L. A., C. Ziehmann, et al. (1999). "Uncertainty dynamics and predictability in chaotic systems." Quarterly Journal of the Royal Meteorological Society 125(560): 2855-2886.

Suarez, M. J. and P. S. Schopf (1988). "A delayed action oscillator for ENSO." Journal of the atmospheric sciences 45(21): 3283-3287.

Tang, Y. and Z. Deng (2010). "Low-dimensional nonlinearity of ENSO and its impact on predictability." Physica D: Nonlinear Phenomena 239(5): 258-268.

Tang, Y. and Z. Deng (2011). "Bred Vector and ENSO Predictability in a Hybrid Coupled Model during the Period 1881-2000." Journal of climate 24(1): 298-314.

Toth, Z. and E. Kalnay (1993). "Ensemble forecasting at NMC: The generation of perturbations." Bulletin of the American Meteorological Society 74(12): 2317-2330.

Trevisan, A., F. Pancotti, et al. (2001). "Ensemble prediction in a model with flow regimes." Quarterly Journal of the Royal Meteorological Society 127(572): 343-358.

Tziperman, E., L. Zanna, et al. (2008). "Nonnormal thermohaline circulation dynamics in a coupled ocean-atmosphere GCM." Journal of Physical Oceanography 38(3): 588-604.

Tziperman, E., S. E. Zebiak, et al. (1997). "Mechanisms of seasonal-ENSO interaction." Journal of the atmospheric sciences 54(1): 61-71.

Vikhliaev, Y., B. Kirtman, et al. (2007). "Decadal North Pacific bred vectors in a coupled GCM." Journal of climate 20(23): 5744-5764.

Wei, M. and Z. Toth (2003). "A New Measure of Ensemble Performance; Perturbation versus Error Correlation Analysis (PECA)." Monthly Weather Review 131(8): 1549-1565.

Xue, Y., M. Cane, et al. (1997). "Predictability of a coupled model of ENSO using singular vector analysis. Part I: Optimal growth in seasonal background and ENSO cycles." Monthly Weather Review 125(9): 2043-2056.

Yang, S., E. Kalnay, et al. (2006). "ENSO bred vectors in coupled ocean-atmosphere general circulation models." Journal of climate 19(8): 1422-1436.

Yang, S. C., E. Kalnay, et al. (2008). "Bred vectors and tropical pacific

forecast errors in the NASA coupled general circulation model." Monthly Weather Review 136(4): 1305-1326.

국 문 초 록

다양한 초기화 과정을 이용한 1991 년부터 2010 년까지 20 년 간 여름철 엘니뇨 예측에 대한 연구가 서울대학교 대기-해양 접합모델을 토대로 진행됐다. 총 14 개의 초기 조건을 생성했는데, 지연 평균 예측(LAF) 기법으로 6 개, 브레드 벡터(BV)와 경험적 특이 벡터(ESV) 기법으로 각각 6 개, 2 개의 초기값을 얻었다. LAF 기법으로는 실제 예측이 시작되기 1~6 일 전 예측을 시작함으로써 각기 다른 초기값을 얻었다. BV 기법에서는 1 달, 3 달 그리고 6 달씩 섭동을 적분한 뒤 자라난 값을 적절히 줄여주는 방법으로 3 가지 섭동(초기 조건)을 구하고, 그것의 거울상을 만들어 총 6 가지 섭동을 만들었다. 나머지 2 개 초기조건은 6 개월 시간 차이가 나는 수온약층 깊이와 해수 표면 온도(SST) 자료를 특이값 분해하여 구했다.

이렇게 해서 실행된 예측의 정확도를 평가하기 위해 니노 인덱스의 상관계수를 계산했다. 그 결과 BV 와 ESV 기법은 LAF 예측력을 뛰어넘었다. BV 초기조건 중에서는 브리딩 기간이 3 달일 때가 가장 예측력이 좋았는데, 특히 중~서태평양에서 효과가

두드러졌다. 엘니뇨해의 BV 섭동 패턴을 분석한 결과 3 개월 적분했을 때 실제 엘니뇨 패턴과 유사한 것이 영향을 미친 것으로 보인다.

BV 초기조건을 ESV 초기조건과 비교하면, 예측 초반에는 BV 기법이, 중반 이후에는 ESV 기법이 우세했다. 이는 스프레드-에러 비율이 시간이 흐를수록 ESV 예측에서 최고 4 배까지 커지기 때문으로 추정된다.

3 달 적분한 BV 와 ESV 를 앙상블 평균하면 초기조건 생성 기법의 예측 기간 의존도가 감소하면서 안정적으로 높은 예측력을 보여주었다. 그러나 눈에 띄는 향상은 나타나지 않았다.

주요어:

엘니뇨, 계절 예측, 지연 평균 예측, 브레드 벡터, 경험적 특이 벡터, 대기-해양 접합모델

학생번호 : 2009-22978